Applied Catalysis B: Environmental 188 (2016) 147–153

Contents lists available at ScienceDirect

Applied Catalysis B: Environmental

journal homepage: www.elsevier.com/locate/apcatb

Plasmonic 'rainbow' photocatalyst with broadband solar light response for environmental applications

Sammy W. Verbruggen[a,b,*], Maarten Keulemans[a,b], Bart Goris[c], Natan Blommaerts[a], Sara Bals[c], Johan A. Martens[b], Silvia Lenaerts[a]

[a] Sustainable Energy, Air & Water Technology, DuEL, Department of Bioscience Engineering, University of Antwerp, Groenenborgerlaan 171, 2020 Antwerp, Belgium
[b] Center for Surface Chemistry and Catalysis, Department of Microbial and Molecular Systems, KU Leuven, Kasteelpark Arenberg 23, 3001 Heverlee, Belgium
[c] EMAT, Department of Physics, University of Antwerp, Groenenborgerlaan 171, 2020 Antwerp, Belgium

ARTICLE INFO

Article history:
Received 28 October 2015
Received in revised form 26 January 2016
Accepted 1 February 2016
Available online 3 February 2016

Keywords:
Photocatalysis
Plasmon (SPR)
Broadband
Solar
Stearic acid

ABSTRACT

We propose the concept of a 'rainbow' photocatalyst that consists of TiO_2 modified with gold-silver alloy nanoparticles of various sizes and compositions, resulting in a broad plasmon absorption band that covers the entire UV–vis range of the solar spectrum. It is demonstrated that this plasmonic 'rainbow' photocatalyst is 16% more effective than TiO_2 P25 under both simulated and real solar light for pollutant degradation at the solid-gas interface. With this we provide a promising strategy to maximize the spectral response for solar to chemical energy conversion.

1. Introduction

Plasmon resonance can be described as an energetic collective oscillation of conduction band electrons on a metal particle. Energetic coupling of this plasmon resonance with a semiconductor is a proven strategy for increasing the spectral response of photoactive materials in the visible light region of the spectrum [1,2]. It has been shown that plasmonic enhancement is maximized when there is a good overlap between the plasmon absorption band and the intensity spectrum of the light source [3,4]. In most cases this requires careful tuning of the plasmonic nanostructures to the utilized light source, which often has a narrow emission spectrum (e.g. lasers, LEDs and monochromatic filtered light). Conversely, for actual solar-driven applications it is more useful to design plasmonic nanostructures that respond to a much broader wavelength range. In that regard the concept of 'broadband plasmons' is beginning to find its way in the field of dye sensitized solar cells (DSSCs) [5–7], where mainly large nanoparticles are used for plasmonic light scattering in order to more effectively utilize incident photons in the solar cell and increase the number of dye excitations. On the other hand the broadband plasmon concept remains unexplored in the field of photocatalytic environmental remediation, where the use of sensitizing dyes is complicated due to severe stability issues [8] and plasmonic enhancement thus takes place through direct interaction with the semiconductor in the absence of sensitizing dyes. In our work the plasmonic nanoparticles are significantly smaller than those envisaged for broadband plasmonic response in DSSCs (i.e. well below 80 nm).

It is known that the plasmon wavelength can be tuned by altering the size or shape of metal nanostructures [9,10]. An alternative versatile way of wavelength tuning is offered by alloying. In the particular case of colloidal gold-silver alloys, plasmon resonance in colloidal solutions can be obtained between ca. 390 nm for pure silver nanoparticles up to 530 nm for pure gold [11]. In this work, we have prepared gold-silver alloys with compositions ranging from 20% to 100% gold, with increments of 10% using a modified Turkevich method. Alloy nanoparticle suspensions with higher silver content do not remain stable for longer periods. So far, only very few reports exist on the photocatalytic activity of gold-silver alloy on TiO_2 nanocomposites, all in liquid phase, such as the production of hydrogen peroxide under UV [12] and the degradation of phenol and rhodamine B under visible light (using high power Xe sources) [13,14]. Applications of plasmonic photocatalysis in gaseous

* Corresponding author at: Sustainable Energy, Air & Water Technology, Department of Bioscience Engineering, University of Antwerp, Groenenborgerlaan 171, 2020 Antwerp, Belgium.
E-mail address: Sammy.verbruggen@uantwerpen.be (S.W. Verbruggen).

http://dx.doi.org/10.1016/j.apcatb.2016.02.002
0926-3373/

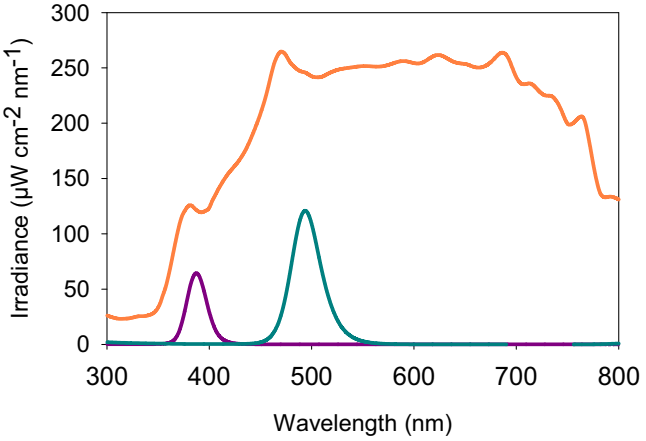

Fig. 1. Absolute irradiance spectra of the different light sources collected at sample distance (5 cm). The integrated intensity (300–800 nm) for the UVA LED source (purple curve) is 1.6 mW/cm^2, for the VIS-490 nm LED source (cyan curve) it is 4.7 mW/cm^2 and for simulated solar light (AM1.5, orange curve) the integrated intensity is ca. 100 mW/cm^2. (For interpretation of the references to color in this figure legend, the reader is referred to the web version of this article.)

environment are altogether scarce [15–18]. Furthermore the concept of broadband plasmons has never been explored in that context. Therefore in this work the photocatalytic activity is evaluated by means of stearic acid degradation at the solid-gas interface, a widely recognized model reaction for organic fouling on solid substrates [19,20].

2. Experimental

2.1. Synthesis of plasmonic 'rainbow' photocatalyst

Colloidal $Au_xAg_{(1-x)}$ nanoparticles were prepared using a modified Turkevich procedure as follows: Appropriate amounts of 0.01 M $HAuCl_4{\cdot}3H_2O$ (Sigma–Aldrich, >99.9%) and 0.01 M $AgNO_3$ (Sigma–Aldrich, >99%) precursor solutions were diluted to a total resulting metal concentration of 0.1 mM to avoid precipitation of AgCl. The solution was stirred vigorously and brought to boil after which 1 mL of a freshly prepared 1 wt% sodium citrate (Sigma–Aldrich, 99%) solution was quickly added and left boiling for exactly 30 min. This procedure was repeated in order to obtain nine colloidal solutions with the gold fraction x varying from 0.2 to 1 with increments of 0.1. For the 'rainbow' sample, equal amounts of each of the nine colloidal gold-silver solutions were mixed together under vigorous stirring.

The plasmonic photocatalysts ($Au_{0.3}Ag_{0.7}$-P25 and 'rainbow'-P25) were prepared by photo-impregnating [21] commercially available P25 (Evonik, surface area $\pm$ 55 m^2 g^{-1}, 80% anatase, 20% rutile) with the corresponding colloidal nanoparticle solution ($Au_{0.3}Ag_{0.7}$ nanoparticle solution or 'rainbow' mixture) under vigorous stirring and UVA illumination (Philips Cleo UVA, 25 W, 365 nm) for 60 min, so the resulting metal loading was 1.5 wt%. The resulting suspension was centrifuged, washed and dried overnight at 383 K.

2.2. Characterization

HAADF-STEM images and EDX maps were acquired using an Osiris electron microscope operated at 200 kV and equipped with a super-X detection system. The total acquisition time for the EDX maps was 3 min. UV–vis spectra of the colloidal alloy suspensions were recorded with a Shimadzu UV–vis 2501PC double beam spectrophotometer. UV–vis absorbance spectra of the plasmonic catalyst powders were collected on the same apparatus,

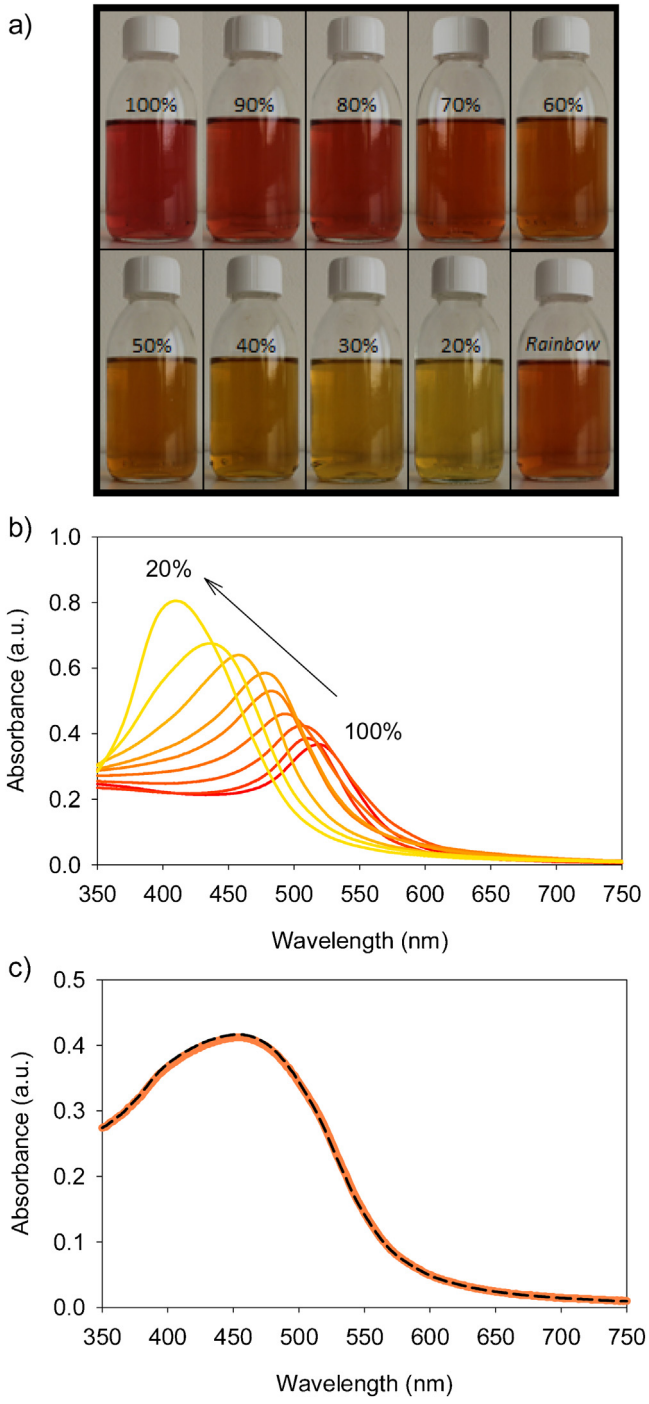

Fig. 2. Optical properties of gold-silver alloy nanoparticle solutions and 'rainbow' sample. (a) Pictures of the colloidal alloy nanoparticle solutions. The percentage indicated on the bottles corresponds to the gold fraction of the gold-silver alloy. (b) UV–vis absorption spectra of the alloy samples in (a). (c) UV–vis absorption spectrum of the 'rainbow' sample (orange curve) and a linear combination of the UV–vis spectra of the composing alloy solutions (black dotted curve). (For interpretation of the references to color in this figure legend, the reader is referred to the web version of this article.)

equipped with a 60 mm $BaSO_4$ coated integrating sphere and a photomultiplier R-446 detector. Dynamic Light Scattering is used for determining the colloidal particle sizes on a BIC 90 Plus apparatus (Brookhaven) with a 15 mW 659 nm laser. Igor Pro (v.6.02) was used to analyze the collected correlation functions. Absolute irradiance measurements of the different light sources are performed with a calibrated Avantes Avaspec 3648 spectrometer.

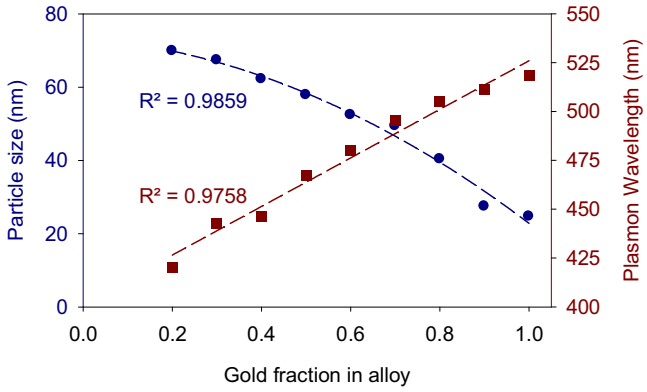

Fig. 3. Observed trends in particle size and plasmon wavelength for gold-silver alloy nanoparticles. The main particle size decreases with increasing gold content of the alloy and can be fitted well by a second order polynomial (blue ●). The plasmon wavelength varies linearly with the gold fraction of the alloy (red ■). (For interpretation of the references to color in the text, the reader is referred to the web version of this article.)

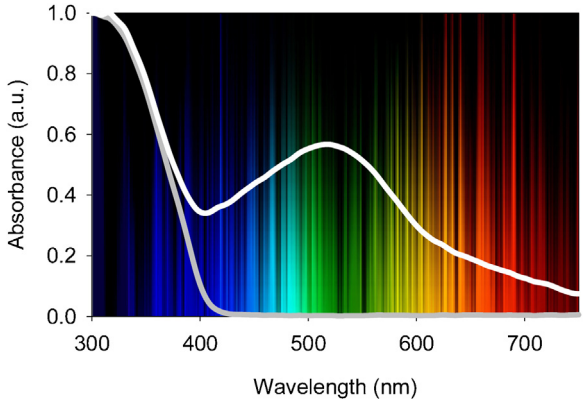

Fig. 5. UV–vis powder spectra of the 'rainbow' photocatalyst (white) and pristine TiO_2 P25 (gray).

2.3. Photocatalytic testing

The photocatalytic activity was evaluated by means of the degradation of stearic acid. The coating and measurement protocols are comparable to our earlier work [3,22]. The photocatalysts were suspended in ethanol (1 wt%) and stirred ultrasonically. 50 μL of the suspension was drop casted on a pre-cleaned silicon wafer (1.5 cm × 3 cm), so the resulting coverage was 88 μg cm^{-2}. Reference samples that only contain metal nanoparticles without TiO_2 are prepared by drop casting a volume of the corresponding colloidal alloy solution containing the equivalent amount of metal nanoparticles on a bare silicon wafer and evaporating the solvent. The resulting metal coverage is thus 1.33 μg cm^{-2}. After drop casting the samples were dried in an oven at 363 K. The investigated samples consist of (i) pristine P25, (ii) P25 modified with 1.5 wt% $Au_{0.3}Ag_{0.7}$ alloy nanoparticles, (iii) the 'rainbow' photocatalyst (containing 1.5 wt% mixed metal alloy nanoparticles), (iv) a blanc silicon wafer, (v) silicon wafer containing the same amount of $Au_{0.3}Ag_{0.7}$ alloy nanoparticles as sample (ii), but without TiO_2 and (vi) silicon wafer containing the same amount and composition of mixed alloy nanoparticles as the 'rainbow' sample, but without TiO_2. The last three samples are used for performing reference experiments to rule out the effect of photolysis (blanc wafer) and stearic acid degradation due to plasmonic heating or direct plasmonic catalysis (silicon wafer containing only noble metal particles but no TiO_2) [23,24]. In all experiments these reference samples showed no activity (see below and in Fig. 6) and are therefore not considered in the further discussion. The sample containing 1.5 wt% $Au_{0.3}Ag_{0.7}$ alloy nanoparticles on P25 was added for comparison purposes as it has its plasmon absorption band maximum exactly at 490 nm, corresponding to λ_{max} of the visible LED light source.

Three different light sources were used for studying the photocatalytic performance of the samples in a lab-environment: UVA (λ_{max} = 385 nm, provided by LEDs), narrow band visible light (λ_{max} = 490 nm, provided by LEDs) and combined simulated solar light (300 W Xe source (Oriel Instruments) equipped with AM1.5 solar simulator). The corresponding incident irradiance spectra and integrated intensity outputs at sample distance (5 cm) are given in Fig. 1. An additional experiment was performed to test the photocatalytic activity of all samples under realistic outdoor conditions.

The degradation of stearic acid was monitored by FTIR on a NicoletTM 380 (Thermo Fisher Scientific) with ZnSe windows at a resolution of 1 cm^{-1} by integration of the wavelength range

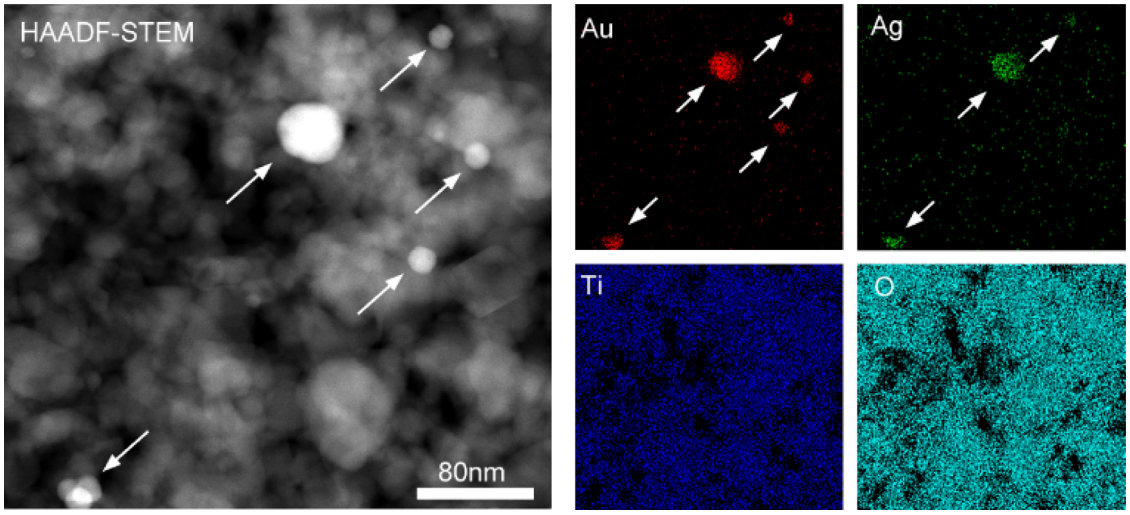

Fig. 4. HAADF-STEM image and elemental maps of 'rainbow' photocatalyst sample. The HAADF-STEM image clearly reveals the presence of metal nanoparticles of different sizes (indicated by white arrows). From the elemental maps obtained with EDX mapping, the TiO_2 support is apparent and the co-presence of gold and silver inside the same nanoparticles supports the concept of alloy formation. Notice the intensity of silver is not equivalent in every particle, as expected from the presence of alloys with different concentrations.

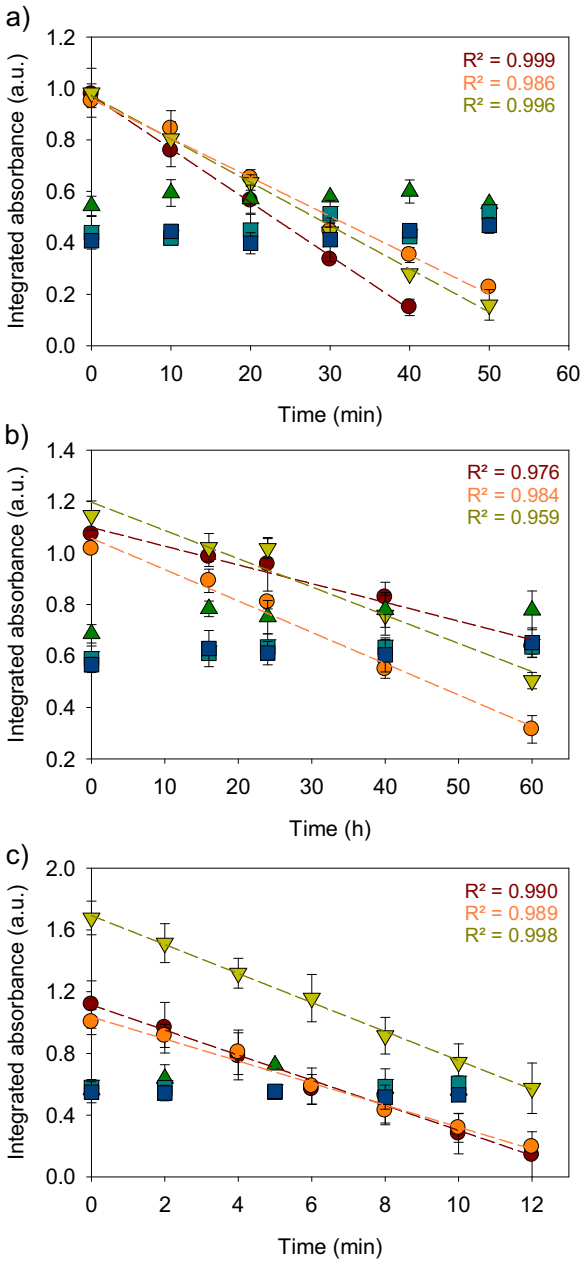

Fig. 6. Stearic acid degradation experiment using different light sources. The different light sources used are (a) UVA LED (λ_{max} = 385 nm), (b) Visible light LED (λ_{max} = 490 nm) and (c) simulated solar light (AM1.5 filter). Tested samples are pristine TiO_2 P25 (red ○), $Au_{0.3}Ag_{0.7}$-P25 (orange ○), 'rainbow'-P25 (yellow ▽), blanc wafer (green △), only $Au_{0.3}Ag_{0.7}$ nanoparticles (cyan □) and only 'rainbow' nanoparticles (blue □). Only the first three samples (those containing TiO_2) show photocatalytic activity and the data points are fitted with a linear regression curve (zero order kinetic behavior). (For interpretation of the references to color in this figure legend, the reader is referred to the web version of this article.)

2800–3000 cm^{-1} [25]. The samples were placed at an angle of 9° to minimize internal reflection effects.

3. Results and discussion

3.1. Plasmonic 'rainbow' photocatalyst

The resulting colloidal solutions appear bright yellow to ruby red (Fig. 2a) and display plasmon resonance over a broad wavelength range (Fig. 2b). The plasmon wavelength varies linearly with the gold fraction of the alloy (Fig. 3, red curve), which is consistent with literature [26,27]. In addition, we noticed for the first time that the particle size gradually increases with decreasing gold content and can be fitted well by a second order polynomial (Fig. 3, blue curve).

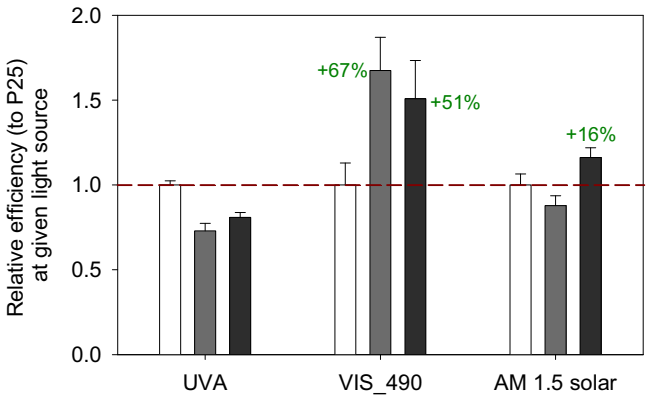

Fig. 7. Relative photocatalytic efficiency of $Au_{0.3}Ag_{0.7}$-P25 (light gray) and the 'rainbow' photocatalyst (dark gray) with regard to pristine TiO_2 P25 (white) under different illumination conditions.

For the 'rainbow' sample, equal amounts of each of the nine colloidal alloy suspensions were mixed and stirred vigorously. The resulting UV–vis spectrum stretches out over a very broad wavelength range. Furthermore, this 'rainbow' sample spectrum is a perfect linear combination of the individual UV–vis spectra of the constituting alloys (Fig. 2c). This is a good indication for the stability of the individual alloy nanoparticles, even when they are intermixed. The 'rainbow' photocatalyst is prepared by depositing the intermixed alloy nanoparticles on the surface of TiO_2 P25 (Evonik) by a photo-impregnation method so that the resulting metal loading is 1.5 wt%. This method enables a homogeneous distribution and retention of the particle size [21]. On the microscopic level the 'rainbow' sample consists of homogeneously distributed gold-silver alloy nanoparticles of various sizes and compositions on the surface of TiO_2 P25 aggregates. This is confirmed by HAADF-STEM imaging and EDX spectroscopy as presented in Fig. 4. Since the intensity in HAADF-STEM scales with the thickness of the sample and with the atomic number Z of the elements that are present, the metallic nanoparticles (indicated by white arrows in Fig. 4) appear with higher intensity in comparison to the TiO_2 support. From the EDX mapping, the co-presence of gold and silver over the entire metal nanoparticle clearly indicates alloy formation.

The resulting absorption spectrum of the 'rainbow' photocatalyst is depicted in Fig. 5 (white curve). The combined plasmon absorption band of all composing alloy nanoparticles stretches out over nearly the entire UV–vis range, in contrast to pristine TiO_2 P25 that has a cut-off in the blue range of the spectrum (gray curve). The maximum of the plasmon absorption band lies in the green range of the spectrum, corresponding to those solar wavelengths with highest intensity output. A strong tail of the plasmon band towards longer wavelengths results in some absorption of red light. This way the entire broad visible light region of the spectrum is spanned by one single catalyst.

3.2. Broadband plasmonic photocatalytic activity at the solid-gas interface

The measured degradation curves obtained with all different samples are plotted in Fig. 6. As mentioned earlier, reference experiments involving a blank wafer or wafers with only metal nanoparticles and no TiO_2 displayed no photocatalytic activity. In all our other experiments the photocatalytic degradation of stearic

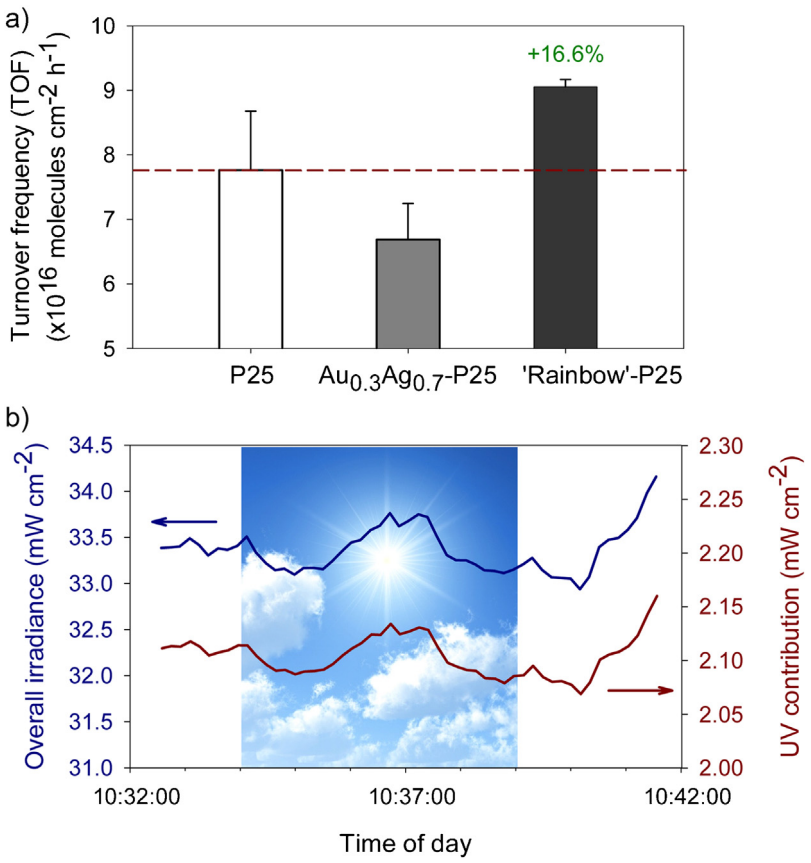

Fig. 8. Real-life photocatalytic experiment. (a) Comparison of the turnover frequency of stearic acid molecules on P25 (white), $Au_{0.3}Ag_{0.7}$-P25 (gray) and the 'rainbow' photocatalyst (dark gray), measured outside under ambient conditions on the Belgian spring day June 12th 2015 between 10:34 a.m. and 10:39 a.m. (b) Variation of the overall incident irradiance (300–800 nm, blue curve) and its UV-contribution (300–400 nm, red curve) during the measurement. (For interpretation of the references to color in this figure legend, the reader is referred to the web version of this article.)

acid obeyed zero order kinetics. Since TiO_2 P25 is the universal photocatalytic reference material, the formal quantum efficiencies of the $Au_{0.3}Ag_{0.7}$-P25 and 'rainbow' photocatalysts are expressed directly with respect to P25 in Fig. 7. Under pure UVA illumination, both metal-modified samples are less efficient than P25. This is most likely the result of metal particles blocking active sites and shielding part of the TiO_2 surface from incoming light. Under narrow-band visible light (490 nm LEDs), both plasmonic samples are significantly more effective than pristine P25, but altogether the efficiencies under visible light remain much smaller than under UV. Although the trace activity of P25 under pure visible light is in itself surprising, it should be technically possible due to the presence of intrinsic surface defect levels (e.g. at the anatase-rutile interface), that have been demonstrated by means of EPR and photoluminescence studies [28,29]. Modification of P25 with plasmonic nanostructures leads to a large improvement of this basal visible light activity. The 'rainbow' photocatalyst is approximately 50% better than P25 and the catalyst containing specifically $Au_{0.3}Ag_{0.7}$ alloy nanoparticles induces an efficiency increase of almost 70%. This is explained by the excellent match between the catalyst's peak plasmon wavelength and λ_{max} of the used light source, both at 490 nm and is a confirmation of some of our earlier work [3]. Interestingly, this high tunability of dedicated gold-silver-alloy-on-TiO_2 catalysts is thus very useful for obtaining visible light photocatalytic activity under predetermined, fixed visible light wavelengths. Under broad-band illumination (simulated sunlight), however, the resulting photocatalytic efficiency of the $Au_{0.3}Ag_{0.7}$-P25 photocatalyst is again comparable to that of unmodified P25. One can indeed expect that plasmonic coupling to one single additional visible light wavelength will not add substantially to the intrinsic photocatalytic efficiency under UV. In contrast, the 'rainbow' photocatalyst is 16% more efficient under this broadband illumination, which can be attributed to simultaneous multiple wavelength plasmonic coupling over nearly the entire UV–vis range.

As a proof of concept, we have also performed a 'real-life application test' under ambient outdoor conditions on a Belgian spring day (Fig. 8). Due to fluctuations in the incident irradiance, we prefer not to refer to the results in terms of efficiencies, but use the turnover frequencies (TOFs) of all samples. The TOF on P25 was 7.76×10^{16} cm^{-2} h^{-1}, the TOF on the $Au_{0.3}Ag_{0.7}$-P25 photocatalyst was a bit lower, 6.69×10^{16} cm^{-2} h^{-1}, while the TOF using the 'rainbow' photocatalyst was significantly higher: 9.05×10^{16} cm^{-2} h^{-1}. Remarkably, the order of reactivity and the relative improvement in activity for the 'rainbow' photocatalyst (16.6%) is identical to the results obtained under simulated solar light under laboratory conditions. This proof of concept thus encourages the further development of this type of plasmonic catalysts for real-life applications.

3.3. Mechanistic considerations

From the current set of experiments we can definitely exclude photolysis, plasmonic heating and direct catalysis on plasmonic particles as the responsible underlying mechanism for the observed photoactivity [23,24]. Three major, mutually non-exclusive mechanistic explanations remain for the observed plasmonic enhancement. Firstly, electrons from an excited plasmonic state can be injected into the TiO_2 conduction band, which

initiates the degradation pathway [30–32]. Secondly, the plasmonic particles can be responsible for strong enhancement of the near-field, which in turn results in more efficient electron-hole pair formation in the TiO_2 substrate in the direct vicinity of the particles [33–35]. A third mechanism that can play to some degree is the extension of the useful optical path of incoming light due to resonant scattering on some of the larger (>50 nm) alloy nanoparticles [36]. The combined effects of UV-driven photo-excitation of TiO_2 and the excitation of plasmon modes under visible light present an additional degree of complexity in pinpointing the exact mechanism under solar light irradiation and is the subject of ongoing research.

Very recently we have been able to demonstrate by means of an EPR study on Au-modified TiO_2 that electron-related species are present in the TiO_2 conduction band upon illumination with (purely visible) green laser light, whereas this is not the case in pristine TiO_2 under the same conditions [37]. This provides experimental evidence for the important role of direct electron injection in the plasmon-mediated reaction mechanism. This is also supported by the recent work of Nishi et al. based on action spectra of Au-Ag alloy on TiO_2 materials [38]. They also confirm the high degree of control that can be achieved over the optical response of this type of material by carefully tuning the alloy composition.

4. Conclusion

We introduce the concept of a plasmonic 'rainbow' photocatalyst consisting of TiO_2 modified with gold-silver alloy nanoparticles of various sizes and compositions. This plasmonic photocatalyst enables simultaneous multiple wavelength absorption over nearly the entire UV–vis range of the spectrum with a maximal response at the highest intensity wavelengths of solar light. The 'rainbow' catalyst shows an increased efficiency toward stearic acid degradation under both narrow-band pure visible light as well as simulated and real broadband sunlight under realistic outdoor conditions (ca. 16–17%). This is the first demonstration of broadband plasmonic photocatalysis for environmental remediation at the solid-gas interface. With this we hope to encourage the further development of plasmonic photocatalysis for environmental applications.

Acknowledgements

S.W.V. and B.G. acknowledge the Research Foundation—Flanders (FWO) for a postdoctoral fellowship. M.K. acknowledges IWT for the doctoral scholarship. S.B. acknowledges the European Research Council (ERC) for financial support through the ERC grant agreement no. 335078-COLOURATOM. J.A.M. acknowledges the Flemish government for long-term structural funding (Methusalem).

References

[1] S. Linic, P. Christopher, D.B. Ingram, Plasmonic-metal nanostructures for efficient conversion of solar to chemical energy, Nat. Mater. 10 (2011) 911–921.
[2] H.A. Atwater, A. Polman, Plasmonics for improved photovoltaic devices, Nat. Mater. 9 (2010) 205–213.
[3] S.W. Verbruggen, M. Keulemans, M. Filippousi, D. Flahaut, G. Van Tendeloo, S. Lacombe, et al., Plasmonic gold–silver alloy on TiO_2 photocatalysts with tunable visible light activity, Appl. Catal. B Environ. 156–157 (2014) 116–121.
[4] D.B. Ingram, P. Christopher, J.L. Bauer, S. Linic, Predictive model for the design of plasmonic metal/semiconductor composite photocatalysts, ACS Catal. 1 (2011) 1441–1447.
[5] A. Dabirian, N. Taghavinia, Theoretical study of light trapping in nanostructured thin film solar cells using wavelength-scale silver particles, ACS Appl. Mater. Interfaces 7 (2015) 14926–14932.
[6] M.D. Brown, T. Suteewong, R.S.S. Kumar, V. D'Innocenzo, A. Petrozza, M.M. Lee, et al., Plasmonic dye-sensitized solar cells using core–shell metal-insulator nanoparticles, Nano Lett. 11 (2011) 438–445.
[7] Q. Xu, F. Liu, Y. Liu, K. Cui, X. Feng, W. Zhang, et al., Broadband light absorption enhancement in dye-sensitized solar cells with Au–Ag alloy popcorn nanoparticles, Sci. Rep. 3 (2013) 2112.
[8] R. Abe, K. Sayama, H. Arakawa, Dye-sensitized photocatalysts for efficient hydrogen production from aqueous I—solution under visible light irradiation, J. Photochem. Photobiol. A: Chem. 166 (2004) 115–122.
[9] L.M. Liz-Marzan, Tailoring surface plasmons through the morphology and assembly of metal nanoparticles, Langmuir 22 (2006) 32–41.
[10] M.A. Garcia, Surface plasmons in metallic nanoparticles: fundamentals and applications, J. Phys. D: Appl. Phys. 44 (2011) 283001 (20p).
[11] S.W. Verbruggen, M. Keulemans, J.A. Martens, S. Lenaerts, Predicting the surface plasmon resonance wavelength of gold–silver alloy nanoparticles, J. Phys. Chem. C 117 (2013) 19142–19145.
[12] D. Tsukamoto, A. Shiro, Y. Shiraishi, Y. Sugano, S. Ichikawa, S. Tanaka, et al., Photocatalytic H_2O_2 production from ethanol/O-2 system using TiO_2 loaded with Au–Ag bimetallic alloy nanoparticles, ACS Catal. 2 (2012) 599–603.
[13] A. Zielińska-Jurek, E. Kowalska, J.W. Sobczak, W. Lisowski, B. Ohtani, A. Zaleska, Preparation and characterization of monometallic (Au) and bimetallic (Ag/Au) modified-titania photocatalysts activated by visible light, Appl. Catal. B: Environ. 101 (2011) 504–514.
[14] Y. Zhu, S. Yang, J. Cai, M. Meng, X. Li, A facile synthesis of $AgxAu_{1-x}/TiO_2$ photocatalysts with tunable surface plasmon resonance (SPR) frequency used for RhB photodegradation, Mater. Lett. 154 (2015) 163–166.
[15] S.W. Verbruggen, TiO_2 photocatalysis for the degradation of pollutants in gas phase: from morphological design to plasmonic enhancement, J. Photochem. Photobiol. C: Photochem. Rev. 24 (2015) 64–82.
[16] Y. Zhang, Z.-R. Tang, X. Fu, Y.-J. Xu, Nanocomposite of Ag–AgBr–TiO2 as a photoactive and durable catalyst for degradation of volatile organic compounds in the gas phase, Appl. Catal. B: Environ. 106 (2011) 445–452.
[17] T. Nogawa, T. Isobe, S. Matsushita, A. Nakajima, Ultrasonication effects on the visible-light photocatalytic activity of Au-modified TiO_2 powder, Mater. Lett. 90 (2013) 79–82.
[18] H. Song, Y.-T. Yu, P. Norby, Efficient complete oxidation of acetaldehyde into CO_2 over Au/TiO2Core–Shell nano catalyst under UV and visible light irradiation, J. Nanosci. Nanotechnol. 9 (2009) 5891–5897.
[19] Y. Paz, Z. Luo, L. Rabenberg, A. Heller, Photooxidative self-cleaning transparent titanium-dioxide films on glass, J. Mater. Res. 10 (1995) 2842–2848.
[20] A. Mills, A. Lepre, N. Elliott, S. Bhopal, I.P. Parkin, S.A. O'Neill, Characterisation of the photocatalyst Pilkington Activ(TM): a reference Film photocatalyst? J. Photochem. Photobiol. A: Chem. 160 (2003) 213–224.
[21] A. Tanaka, A. Ogino, M. Iwaki, K. Hashimoto, A. Ohnuma, F. Amano, et al., Gold–titanium(IV) oxide plasmonic photocatalysts prepared by a colloid-photodeposition method: correlation between physical properties and photocatalytic activities, Langmuir 28 (2012) 13105–13111.
[22] S. Deng, S.W. Verbruggen, S. Lenaerts, J.A. Martens, S. Van den Berghe, K. Devloo-Casier, et al., Controllable nitrogen doping in as deposited Ti film and its effect on post deposition annealing, J. Vac. Sci. Technol. A 32 (2014) 01A123.
[23] J.R. Adleman, D.A. Boyd, D.G. Goodwin, D. Psaltis, Heterogenous catalysis mediated by plasmon heating, Nano Lett. 9 (2009) 4417–4423.
[24] M.J. Kale, T. Avanesian, P. Christopher, Direct photocatalysis by plasmonic nanostructures, ACS Catal. 4 (2014) 116–128.
[25] E. Allain, S. Besson, C. Durand, M. Moreau, T. Gacoin, J.P. Boilot, Transparent mesoporous nanocomposite films for self-cleaning applications, Adv. Funct. Mater. 17 (2007) 549–554.
[26] S. Link, M.A. El-Sayed, Size and temperature dependence of the plasmon absorption of colloidal gold nanoparticles, J. Phys. Chem. B 103 (1999) 4212–4217.
[27] S. Link, Z.L. Wang, M.A. El-Sayed, Alloy formation of gold-silver nanoparticles and the dependence of the plasmon absorption on their composition, J. Phys. Chem. B 103 (1999) 3529–3533.
[28] Y. Yang, T. Zhang, L. Le, X. Ruan, P. Fang, C. Pan, et al., Quick and facile preparation of visible light-driven TiO_2 photocatalyst with high absorption and photocatalytic activity, Sci. Rep. 4 (2014) 7045.
[29] F.J. Knorr, D. Zhang, J.L. McHale, Influence of TiCl4 treatment on surface defect photoluminescence in pure and mixed-phase nanocrystalline TiO_2, Langmuir 23 (2007) 8686–8690.
[30] Y. Tian, T. Tatsuma, Mechanisms and applications of plasmon-induced charge separation at TiO_2 films loaded with gold nanoparticles, J. Am. Chem. Soc. 127 (2005) 7632–7637.
[31] C.G. Silva, R. Juárez, T. Marino, R. Molinari, H. García, Influence of excitation wavelength (UV or visible light) on the photocatalytic activity of titania containing gold nanoparticles for the generation of hydrogen or oxygen from water, J. Am. Chem. Soc. 133 (2011) 595–602.
[32] E. Kowalska, O.O.P. Mahaney, R. Abe, B. Ohtani, Visible-light-induced photocatalysis through surface plasmon excitation of gold on titania surfaces, Phys. Chem. Chem. Phys. 12 (2010) 2344–2355.
[33] K. Awazu, M. Fujimaki, C. Rockstuhl, J. Tominaga, H. Murakami, Y. Ohki, et al., A plasmonic photocatalyst consisting of sliver nanoparticles embedded in titanium dioxide, J. Am. Chem. Soc. 130 (2008) 1676–1680.
[34] D.B. Ingram, S. Linic, Water splitting on composite plasmonic-metal/semiconductor photoelectrodes: evidence for selective

plasmon-induced formation of charge carriers near the semiconductor surface, J. Am. Chem. Soc. 133 (2011) 5202–5205.
[35] Z.W. Liu, W.B. Hou, P. Pavaskar, M. Aykol, S.B. Cronin, Plasmon resonant enhancement of photocatalytic water splitting under visible illumination, Nano Lett. 11 (2011) 1111–1116.
[36] D.D. Evanoff, G. Chumanov, Synthesis and optical properties of silver nanoparticles and arrays, ChemPhysChem 6 (2005) 1221–1231.
[37] I. Caretti, M. Keulemans, S.W. Verbruggen, S. Lenaerts, S. Van Doorslaer, Light-induced processes in plasmonic gold/TiO_2 photocatalysts studied by electron paramagnetic resonance, Top Catal. 58 (2015) 776–782.
[38] H. Nishi, T. Torimoto, T. Tatsuma, Wavelength- and efficiency-tunable plasmon-induced charge separation by the use of Au–Ag alloy nanoparticles, Phys. Chem. Chem. Phys. 17 (2015) 4042–4046.